Available online at www.sciencedirect.com

ScienceDirect

IFAC PapersOnLine 59-20 (2025) 154–161

Fixed-Time Composite Neuro-Adaptive Prescribed Performance Control of Spacecraft Considering Model Uncertainties and External Disturbances

Mostafa Ezabadi * **Seyyed Ali Emami** * **Paolo Castaldi** **

* *Department of Aerospace Engineering, Sharif University of Technology, Tehran, Iran.*
** *Department of Electrical, Electronic and Information Engineering "Guglielmo Marconi", University of Bologna, Via Dell'Università 50, Cesena, Italy*

Abstract: This paper presents a prescribed performance attitude control strategy for spacecraft that handles modeling uncertainties and external disturbances. A novel performance function, based on fixed-time stability, is introduced, where the convergence time of the tracking errors to a neighborhood of zero is pre-assigned by the user, independent of the initial conditions. A backstepping control method is employed to design a state feedback controller with a finite-time differentiator incorporated to prevent term explosion during the backstepping process. A combination of a neural network and a disturbance observer is used to address modeling uncertainties and external disturbances alongside composite learning to enhance estimation accuracy. The stability of the proposed control system is rigorously validated through the Lyapunov method. Simulation results demonstrate that the control strategy successfully drives the spacecraft's state variable errors to the vicinity of zero within the specified time frame, even in the presence of uncertainties and disturbances.

Keywords: Fixed-Time Control, Composite Learning, Prescribed Performance Control, Spacecraft Attitude Control, Finite-Time Differentiator

1. INTRODUCTION

The precise control of spacecraft attitude is paramount for the success of numerous space missions. From maintaining stable communication links (Horri and Palmer, 2012) to achieving accurate pointing for scientific observations (Doruk, 2008), the ability to manipulate and maintain a spacecraft's orientation is crucial. Traditional attitude control methods often struggle with uncertainties, disturbances, and actuator limitations. Prescribed performance control (PPC) emerges as a powerful technique addressing these challenges by guaranteeing specific performance metrics, such as overshoot, settling time, and steady-state error, within predefined bounds (Gui et al., 2024).

Convergence time is a critical parameter that must be carefully considered in the design of control systems. In many space missions, the use of asymptotic stability does not adequately meet mission requirements, as it is essential that the mission be completed within a constrained time frame. To address this limitation, the concept of finite-time stability was introduced (Bhat and Bernstein, 2000), which has been extensively applied in the problem of spacecraft attitude control (Ezabadi and Emami, 2024). However, a key challenge with this approach is its dependence on the initial conditions, as the convergence time varies with the initial state of the system. To overcome this issue, the concept of fixed-time stability was proposed (Polyakov, 2011), with the aim of eliminating the dependency of convergence time on the initial conditions. Since the introduction of fixed-time stability, this method has been widely utilized in the design of satellite attitude control systems (Liu et al., 2024).

Early research in spacecraft attitude control often relied on simpler methods such as PID controllers (Xiang et al., 2019). However, these methods proved inadequate in handling the complexities of spacecraft dynamics, including nonlinearities, uncertainties, and external disturbances. Furthermore, actuator limitations, such as saturation, posed significant challenges (Shao et al., 2018). The need for more robust and reliable control strategies led to the development and exploration of advanced techniques, including prescribed performance control. The initial applications of PPC in spacecraft attitude control were focused on establishing the theoretical framework and demonstrating its feasibility (Hu et al., 2017a). This involved transforming the original attitude tracking error dynamics into a state-constrained equivalent, allowing for the enforcement of specific performance constraints (Shao et al., 2018). However, these early approaches often faced limitations in handling unknown disturbances effectively. In a recent study (Gao et al., 2021b), an attitude control strategy based on Barrier Lyapunov functions was derived, utilizing transform error and incorporating a finite-time prescribed performance function to allow for the achievement of stability within a predefined time. Additionally, some researchers have investigated model-free PPC techniques to improve the practical applicability of this

10.1016/j.ifacol.2025.11.142

approach (Luo et al., 2018). A model-free PPC method, characterized by low complexity, was proposed, capable of satisfying prescribed performance objectives without the need for knowledge of system dynamics or external disturbances. This concept was later extended to flexible spacecraft by developing a two-layer model-free PPC method (Hu et al., 2020). In addition, (Golestani et al., 2022) investiages the problem of prescribed performance attitude stabilization of a rigid body under physical limitations.

Backstepping control (Gao et al., 2021a; Guan et al., 2023) is a widely used technique in PPC due to its ability to handle nonlinear systems systematically. It involves recursively designing a controller by adding virtual control inputs to stabilize the system's states. The combination of backstepping with prescribed performance functions ensures that the tracking errors remain within predefined bounds (Guan et al., 2023). currently, an adaptive fault-tolerant controller is introduced that integrates backstepping control with Barrier Lyapunov functions, ensuring robust performance in attitude tracking for spacecraft even in the presence of actuator faults and input saturation (Hu et al., 2017b).

In this paper, we propose a novel attitude control strategy for spacecraft, integrating prescribed performance control with fixed-time stability to address modeling uncertainties and external disturbances effectively. Unlike traditional methods that rely on asymptotic convergence, our approach allows for the pre-assignment of convergence time, independent of the system's initial conditions. The control design leverages a backstepping method to ensure robustness, complemented by a finite-time differentiator to mitigate potential term explosions during the process. Furthermore, a combination of neural networks and disturbance observers is utilized to enhance the accuracy of disturbance estimation.

The structure of the present paper is organized as follows: Section 2 provides the background, which includes notations, definitions and basic lemmas. A detailed overview of mathematical modeling and problem formulation is provided in Section 3. The results of the stability analysis using Lyapunov method are presented in section 4, supporting the effectiveness of the proposed approach in providing bounded tracking errors. Simulation results validating the proposed control strategy against a range of scenarios are given in Section 5. Finally, Section 6 concludes the paper, summarizing key findings and potential future research directions.

2. BACKGROUND

2.1 Definitions and Lemmas

Lemma 1. (Zuo (2015)). Consider a dynamic system $\dot{x} = f(x)$. If a Lyapunov function $V(x) : \mathbb{R}^n \to \mathbb{R}^+ \cup \{0\}$ satisfies the following condition:

$$\dot{V}(x) \le -\alpha V^{\frac{m}{n}}(x) - \beta V^{\frac{p}{r}}(x) \tag{1}$$

where α and β are positive constants, and $m, n, p, r \in \mathbb{R}^+$ are odd integers satisfying $m > n$ and $r > p$, then the system is fixed-time stable. Moreover, the reaching time is bounded by:

$$T < T_{\max} = \frac{r}{r-p}\left[\frac{1}{\sqrt{\alpha\beta}}\tan^{-1}\left(\sqrt{\frac{\alpha}{\beta}}\right) + \frac{1}{\alpha\upsilon}\right] \tag{2}$$

Here, $\upsilon = \frac{r(m-n)}{n(r-p)} \le 1$.

Lemma 2. (Zuo et al. (2017)). For $x_i \in \mathbb{R}^+ \cup \{0\}, i = 1, \dots, n$, and $\eta > 0$, the following inequalities are hold:

$$\begin{cases} \sum_{i=1}^{n} x_i^{\eta} \ge \left(\sum_{i=1}^{n} x_i\right)^{\eta} & \eta \in (0,1] \\ \sum_{i=1}^{n} x_i^{\eta} \ge n^{1-\eta}\left(\sum_{i=1}^{n} x_i\right)^{\eta} & \eta \in [1,\infty) \end{cases} \tag{3}$$

Definition 1. For $\iota = \left[\iota_1 \ \dots \ \iota_n\right]^T$, $\iota^{[r]}$ is defined as follows:

$$\iota^{[\eta]} = \left[|\iota_1|^{\eta}\operatorname{sign}(\iota_1) \ \dots \ |\iota_n|^{r}\operatorname{sign}(\iota_n)\right]^T \tag{4}$$

Corollary 1. Using Definition 1, for $\iota = \left[\iota_1 \ \dots \ \iota_n\right]^T$, we have:

$$\begin{aligned} \iota^T\iota^{[\eta]} &= \iota_1|\iota_1|^{\eta}\operatorname{sign}(\iota_1) + \dots + \iota_1|\iota_n|^{\eta}\operatorname{sign}(\iota_n) \\ &= |\iota_1|^{1+\eta} + \dots + |\iota_n|^{1+\eta} = (\iota_1^2)^{\frac{1+\eta}{2}} + \dots + (\iota_n^2)^{\frac{1+\eta}{2}} \\ &= \left(\sum_{i=1}^{n}\iota_i^2\right)^{\frac{1+\eta}{2}} \end{aligned} \tag{5}$$

By Lemma 2, for $r > 0$, the following inequlities hold:

$$\begin{cases} \iota^T\iota^{[\eta]} \ge \left(\iota^T\iota\right)^{\frac{1+\eta}{2}} & \eta \in (0,1] \\ \iota^T\iota^{[\eta]} \ge n^{1-\eta}\left(\iota^T\iota\right)^{\frac{1+\eta}{2}} & \eta \in [1,\infty) \end{cases} \tag{6}$$

Definition 2. (Modified Young's Inequality). For two vectors $\iota_1, \iota_2 \in \mathbb{R}^n$ and a positive constant $c_y \in \mathbb{R}^+$, the following inequality is satisfied:

$$\iota_1^T\iota_2 \le \frac{c_y}{2}\iota_1^T\iota_1 + \frac{1}{2c_y}\iota_2^T\iota_2 \tag{7}$$

2.2 Prescribed Performance Control

In the design of control systems, both steady-state and transient response behaviors are critical for system performance. The prescribed performance control framework, in addition to ensuring desired steady-state performance, explicitly addresses the transient response characteristics. This section, along with the subsequent discussion, will delineate the fundamental design requirements inherent to the prescribed performance control approach.

Performance Function

Definition 3. A performance function $\rho : \mathbb{R}^+ \to \mathbb{R}^+$ is a smooth, positive, and strictly decreasing function. Additionally, it satisfies $\lim_{t\to\infty}\rho(t) = \rho_\infty$, where $\rho_\infty > 0$ represents the maximum permissible tracking error in the steady-state (Bechlioulis and Rovithakis, 2008).

One of the most widely employed performance functions is given by (Bechlioulis and Rovithakis, 2008):

$$\rho(t) = (\rho_0 - \rho_\infty)e^{-lt} + \rho_\infty \tag{8}$$

where ρ_0 denotes the initial value of the performance function at $t = 0$, and $l > 0$ is a design parameter. By using the performance function, it ensures that the tracking error satisfies the following boundary condition:

$$\begin{cases} e(0) \ge 0 : -\delta\rho(t) < e(t) < \rho(t) \\ e(0) < 0 : -\rho(t) < e(t) < \delta\rho(t) \end{cases} \tag{9}$$

for all $t > 0$, where $0 \le \delta \le 1$.

Error Transformation The introduction of a performance function imposes a constraint on the design of the control system. The existence of such constraints complicates the design process, necessitating more sophisticated methodologies. In the literature on prescribed performance control, an error transformation is employed to effectively transform the constrained system into an unconstrained one:

$$e(t) = \rho(t) S(\varepsilon) \tag{10}$$

where ε and S are the transformed error and transformation function, respectively.

3. SYSTEM DESCRIPTION AND PROBLEM FORMULATION

3.1 Spacecraft Attitude Equation

To develop the spacecraft attitude dynamics, three key coordinate systems are considered: the inertial frame, the body frame, and the orbital reference frame. The orientation of the spacecraft's body frame relative to the orbital reference frame is efficiently represented using quaternions, offering a robust mathematical framework for describing the satellite's rotational behavior. The attitude dynamics of the spacecraft can be described by the following system of equations:

$$\dot{\bar{q}}_I(t) = \frac{1}{2} E(\bar{q}_I) \omega \tag{11}$$

$$J\dot{\omega}(t) = -\omega^{\times} J\omega + u + d(t) \tag{12}$$

In Equation (11), $\bar{q}_I = \left[q_I^T \ q_4\right]^T$ represents the spacecraft's attitude orientation relative to the inertial frame. Here, $q_I = \left[q_1 \ q_2 \ q_3\right]^T \in \mathbb{R}^3$ denotes the vector component, and $q_4 \in \mathbb{R}$ is the scalar component of the quaternion. The matrix $E(\bar{q})$ is given by:

$$E(\bar{q}_I) = \left[\left(q_4 I_3 + q_I^{\times}\right)^T \ -q_I^T\right]^T \tag{13}$$

The angular velocity $\omega \in \mathbb{R}^3$ represents the spacecraft's angular velocity with respect to the inertial frame, expressed in the body frame. Equation (12) describes the spacecraft's rotational dynamics, where $J = J_0 + \Delta J$ is the inertia matrix. Here, J_0 represents the nominal moment of inertia matrix, and ΔJ accounts for uncertainties in the inertia matrix. The term u denotes the control input, while $d(t)$ represents external disturbances, such as the gravity gradient and aerodynamic drag. A detailed explanation of how to compute external disturbances resulting from gravity gradient and aerodynamic drag can be found in Baldi et al. (2019).

Relative Attitude Equation Let ω_{BL} represent the angular velocity of the body frame relative to the inertial frame, expressed in the body frame. Additionally, let ω_r denote the angular velocity of the reference frame relative to the inertial frame, expressed in the reference frame, which remains constant for circular orbits. The following equation relates these angular velocities to the angular velocity of the body frame relative to the inertial frame:

$$\omega = \omega_{BL} + C(\bar{q}_{BL}) \omega_r \tag{14}$$

In this context, $\bar{q}_{BL}$ denotes the orientation of the body frame relative to the reference frame. The term $C(\bar{q}_{BL}) = C = \left(q_{BL_4}^2 - q_{BL}^T q_{BL}\right) I_3 + 2q_{BL} q_{BL}^T - 2q_{BL_4} q_{BL}^{\times}$ represents the rotation matrix that converts coordinates from the reference frame to the body frame. By substituting Equation (14) into Equation (12) and simplifying the resulting expression, we arrive at:

$$\begin{cases} \dot{\bar{q}}_{BL}(t) = \frac{1}{2} E(\bar{q}_{BL}) \omega_{BL} \\ \dot{\omega}_{BL}(t) = f + gu + \Delta + D \end{cases} \tag{15}$$

The definitions of the terms f, g, Δ, and D are provided as follows:

$$f = J_0^{-1} \Big\{ J_0 \left(\omega_{BL}^{\times} C\omega_r - C\dot{\omega}_r\right) - \left(\omega_{BL} + C\omega_r\right)^{\times} J_0 \left(\omega_{BL} + C\omega_r\right) \Big\} \tag{16a}$$

$$g = J_0^{-1} \tag{16b}$$

$$\begin{aligned} \Delta = \left(J_0^{-1} + \Delta_J\right) \Big\{ \Delta J \left(\omega_{BL}^{\times} C\omega_r - C\dot{\omega}_r\right) - \left(\omega_{BL} + C\omega_r\right)^{\times} \Delta J \left(\omega_{BL} + C\omega_r\right) \Big\} + \Delta_J \Big\{ u + J_0 \left(\omega_{BL}^{\times} C\omega_r - C\dot{\omega}_r\right) \\ - \left(\omega_{BL} + C\omega_r\right)^{\times} J_0 \left(\omega_{BL} + C\omega_r\right) \Big\} \end{aligned} \tag{16c}$$

$$D = \left(J_0^{-1} + \Delta_J\right) d(t) \tag{16d}$$

Here, J_0 refers to the known component of the spacecraft's moment of inertia, while ΔJ represents the unknown part. Additionally, Δ_J is defined as (Ma, 2012):

$$\Delta_J = -J_0^{-1} \Delta J \left(I_3 + J_0^{-1} \Delta J\right)^{-1} J_0^{-1} \tag{17}$$

Assumption 1. The subsequent analysis is based on the following assumptions:

- The uncertainty in the inertia matrix, ΔJ, external disturbances, d, and its first derivative, $\dot{d}$, are bounded (Yao, 2021).
- The desired trajectory for the spacecraft's Euler angles, θ_d, and its time derivative are both bounded.

Relative Attitude Error Kinematics Let $\bar{q}_d = \left[q_d^T \ q_{d_4}\right]^T \in \mathbb{R}^4$ represent the desired attitude quaternion, and let $\omega_d \in \mathbb{R}^3$ represent the desired angular velocity vector. Both are defined relative to the transformation between the reference frame and the body-fixed frame. These reference parameters are derived analytically from a given set of Euler angles that specify the desired orientation. The attitude tracking error and angular velocity tracking error are then formally defined as follows:

$$\bar{q}_e = \bar{q}_{BL} \otimes \bar{q}_d^* \tag{18a}$$

$$\omega_e = \omega_{BL} - \omega_d \tag{18b}$$

In this context, $\otimes$ signifies the quaternion product, while $\bar{q}_d^* = \left[-q_d \ q_{d_4}\right]^T \in \mathbb{R}^4$ denotes the conjugate of the quaternion $\bar{q}_d$.

Remark 1. This paper proposes a control system that combines a neural network with a disturbance observer to mitigate the effects of modeling inaccuracies and external disturbances. The neural network is utilized to address system model uncertainties, while the disturbance observer compensates for external disturbances and estimation errors introduced by the neural network. Specifically, the disturbance observer ensures that the uncertain dynamics fall within the domain of attraction of the neural network, which subsequently compensates for state-dependent uncertainties. This approach enables the control system to deliver robust performance in the presence of uncertainties and disturbances, effectively managing the spacecraft's attitude dynamics (Emami et al., 2023).

4. MAIN RESULTS

4.1 Fixed-Time Performance Function

Given the time-critical nature of many space missions, it is essential not only to regulate the transient response but also to guarantee finite-time convergence of the tracking error within the prescribed allowable bounds. To address this, the present paper introduces a novel performance function grounded in fixed-time stability:

$$\dot{\rho} = \begin{cases} -c\left[(\rho-\rho_\infty)^{2\xi_1-1} + (\rho-\rho_\infty)^{2\xi_2-1}\right] & t \le T \\ 0 & t > T \end{cases} \tag{19}$$

where $\xi_1 = \frac{m}{n} > 1$ and $\xi_2 = \frac{p}{r} > 0.5$. Moreover, c is defined as follows:

$$c = \frac{1}{T}\left(\frac{r}{r-p}\right)\left[\frac{1}{\sqrt{2^{\xi_1+\xi_2}}}\tan^{-1}\left(\sqrt{2^{\xi_1-\xi_2}}\right) + \frac{1}{2^{\xi_1}\upsilon}\right] \tag{20}$$

Theorem 1. The proposed performance function introduced in Equation (19) reaches its steady-state value at the user-specified time, T.

Proof. Consider the following Lyapunov function candidate:

$$V_\rho = \frac{1}{2}(\rho-\rho_\infty)^2 \tag{21}$$

The time derivative of V_ρ is given by:

$$\begin{aligned} \dot{V}_\rho &= \dot{\rho}(\rho-\rho_\infty) = -c(\rho-\rho_\infty)^{2\xi_1} - c(\rho-\rho_\infty)^{2\xi_2} \\ &\le -\alpha\left[\frac{1}{2}(\rho-\rho_\infty)^2\right]^{\xi_1} - \beta\left[\frac{1}{2}(\rho-\rho_\infty)^2\right]^{\xi_2} \\ &\le -\alpha V_\rho^{\xi_1} - \beta V_\rho^{\xi_2} \end{aligned} \tag{22}$$

where $\alpha = 2^{\xi_1}c$ and $\beta = 2^{\xi_2}c$. Consequently, the upper bound on the convergence time can be derived as follows:

$$\begin{aligned} T &< \left(\frac{r}{r-p}\right)\left[\frac{1}{c\sqrt{2^{\xi_1+\xi_2}}}\tan^{-1}\sqrt{2^{\xi_1-\xi_2}} + \frac{1}{c\left(2^{\xi_1}\upsilon\right)}\right] \\ &= \frac{1}{c}\left(\frac{r}{r-p}\right)\left[\frac{1}{\sqrt{2^{\xi_1+\xi_2}}}\tan^{-1}\sqrt{2^{\xi_1-\xi_2}} + \frac{1}{2^{\xi_1}\upsilon}\right] \\ &= T \end{aligned} \tag{23}$$

which completes the proof.

4.2 Finite-Time Differentiator

This paper leverages the backstepping method for the design of the spacecraft attitude control system. A key consideration is that this approach necessitates the computation of the time derivative of the virtual control, a process that is both computationally intensive and non-trivial. To address this inherent challenge, several techniques have been proposed, including command-filtered backstepping (Farrell et al., 2009) and finite-time differentiators (FD) (Bu et al., 2018). In this work, a finite-time differentiator is employed, as it offers a distinct advantage over command-filtered backstepping: it ensures that all state variables remain confined within predefined, permissible bounds:

$$\begin{cases} \dot{\upsilon}_1 = \upsilon_2 \\ \dot{\upsilon}_2 = R^2\left[-a_1\tanh(\upsilon_1-\alpha_h) - a_2\tanh\left(\frac{\upsilon_2}{R}\right)\right] \end{cases} \tag{24}$$

In this context, α_h represents the virtual control, which elegantly serves as the input to the finite-time differentiator. The system states, denoted by υ_1 and υ_2, correspond to the estimates of α_h and its time derivative $\dot{\alpha}_h$, respectively. Moreover, the positive design parameters a_1, a_2, and R are carefully selected to regulate the system's dynamic behavior. To quantify the estimation error, we define $\delta_h = \upsilon_1 - \alpha_h$, and it can be shown that there exists a constant $\bar{\delta}_h \in \mathbb{R}^+$ such that $|\delta_h| \le \bar{\delta}_h$.

Remark 2. As previously mentioned, this paper employs a finite-time differentiator to mitigate the effect of explosion of terms. Compared to the command-filtered backstepping approach, the proposed method offers a framework that maintains all system states within the defined error bounds, whereas the command-filtered backstepping method only guarantees that the first state remains within the prescribed error bound. Moreover, in the command-filtered backstepping method, appropriate auxiliary variables must be defined to compensate for the filtering effect, whereas the finite-time differentiator method does not require the use of such auxiliary variables.

4.3 Composite Learning method

Modeling uncertainties and external disturbances is addressed through a hybrid approach that combines a neural network with a disturbance observer. To enhance the accuracy of estimating these unknown parameters, a composite learning method is employed. In this approach, two training signals—the tracking error and the estimation error—are utilized to update the neural network weights and refine the disturbance observer. The estimation error signal is generated via the design of a state observer. The proposed state observer for angular velocity in this work is as follows:

$$\dot{\hat{\omega}}_{BL} = f + gu + \hat{\Delta} + \hat{D} - k_{e_\omega}\tilde{\omega}_{BL} - k_{e_\omega}\tilde{\omega}_{BL}^{[\eta_1]} - k_{e_\omega}\tilde{\omega}_{BL}^{[\eta_2]} \tag{25}$$

where $\eta_1 = 2m_\omega/n_\omega - 1 \in \mathbb{R}^+$ and $\eta_2 = 2p_\omega/r_\omega - 1 \in \mathbb{R}^+$.

4.4 Prescribed Performance Control Design

The following theorem forms the foundation of this work.

Theorem 2. For the spacecraft dynamics described in Equation 1, if the control input u is designed as:

$$u = g^{-1}\left(-f_\omega - \hat{\Delta} - \hat{D} - \ell_\omega - k_\omega\zeta_\omega^{-1}\varepsilon_\omega + \dot{\upsilon}_\omega + \dot{\omega}_d\right) \tag{26}$$

then, all spacecraft states will remain bounded. The specific definitions of the variables involved will be provided in subsequent sections.

Proof. The transformed error of the quaternion and the angular velocity error vectors is defined as follows:

$$\varepsilon_i = \frac{1}{2}\ln\left(\frac{1+z_i}{1-z_i}\right),\ i = q,\omega \tag{27}$$

where $z_q = \frac{q_e}{\rho_q} \in \mathbb{R}^3$ and $z_\omega = \frac{e_\omega}{\rho_\omega} \in \mathbb{R}^3$. Moreover, the time derivative of ε_q and ε_ω are given by:

$$\dot{\varepsilon}_q = \zeta_q\left(\dot{q}_e + \ell_q\right) \tag{28a}$$

$$\dot{\varepsilon}_\omega = \zeta_\omega\left(\dot{e}_\omega + \ell_\omega\right) \tag{28b}$$

Here, $e_\omega = \omega_e - \upsilon_\omega$, where υ_ω is obtained from Equation (24), and $\zeta_i \in \mathbb{R}^{3\times3}, i = q,\omega$ is a positive-definite symmetric matrix, defined as follows ($j = 1,2,3$):

$$\zeta_q(j,j) = \frac{\rho_q}{\rho_q^2 - q_e^2(j)},\ \zeta_\omega(j,j) = \frac{\rho_\omega}{\rho_\omega^2 - e_{\omega_e}^2(j)} \tag{29}$$

In addition, $\ell_i \in \mathbb{R}^3, i = q,\omega$ is given by ($j = 1,2,3$):

$$\ell_q(j) = -\frac{\dot{\rho}_q}{\rho_q}q_e(j),\ \ell_\omega(j) = -\frac{\dot{\rho}_\omega}{\rho_\omega}e_\omega(j) \tag{30}$$

Furthermore, based on the variable definitions provided in the preceding sections, the angular velocity error can be expressed as:

$$\omega_e = \alpha_\omega + e_\omega + \delta_\omega \tag{31}$$

where $\delta_\omega = \upsilon_\omega - \alpha_\omega$, which is bounded.

Step 1: Consider the following Lyapunov function candidate:

$$V_q = \frac{1}{2}\varepsilon_q^T\varepsilon_q \tag{32}$$

The time derivative of V_q is given by:

$$\begin{aligned}\dot{V}_q &= \varepsilon_q^T\dot{\varepsilon}_q = \varepsilon_q^T\zeta_q\left(\dot{q}_e + \ell_q\right)\\ &= \varepsilon_q^T\zeta_q\left(E(\bar{q}_e)\omega_e + \ell_q\right)\\ &= \varepsilon_q^T\zeta_q\left(E(\bar{q}_e)\alpha_\omega + E(\bar{q}_e)e_\omega + E(q_e)\delta_\omega + \ell_q\right)\end{aligned} \tag{33}$$

By designing α_ω as:

$$\alpha_\omega = E^{-1}(\bar{q}_e)\left(-\ell_q - k_q\zeta_q^{-1}\varepsilon_q\right) \tag{34}$$

the expression for $\dot{V}_q$ simplifies as follows:

$$\dot{V}_q = \varepsilon_q^T\left(\zeta_q E(\bar{q}_e)e_\omega + \zeta_q E(\bar{q}_e)\delta_\omega - k_q\varepsilon_q\right) \tag{35}$$

Assuming that e_ω is bounded, we obtain:

$$\zeta_q E(\bar{q}_e)e_\omega + \zeta_q E(\bar{q}_e)\delta_\omega \le \varkappa \tag{36}$$

By applying the modified Young's inequality, we obtain:

$$\varepsilon_q^T\left\{\zeta_q E(\bar{q}_e)e_\omega + \zeta_q E(\bar{q}_e)\delta_\omega\right\} \le \frac{\delta_{\varepsilon_q}}{2}\varepsilon_q^T\varepsilon_q + \frac{1}{2\delta_{\varepsilon_q}}\varkappa^T\varkappa \tag{37}$$

where $\delta_{\varepsilon_q} \in \mathbb{R}^+$ is a design constant. Substituting Equation (37) into Equation (33), the following expression is obtained:

$$\dot{V}_q \le -k_q' V_q + c_q \tag{38}$$

where $k_q' = \min\left(2k_q - \delta_{\varepsilon_q}\right)$ with $k_q > \frac{\delta_{\varepsilon_q}}{2}$ and $c_q = \frac{\varkappa^T\varkappa}{2\delta_{\varepsilon_q}}$.

Step 2: Consider the following Lyapunov function:

$$V_\omega = \frac{\varepsilon_\omega^T\varepsilon_\omega}{2} + \frac{k_{p_\omega}}{2}\tilde{\omega}_{BL}^T\tilde{\omega}_{BL} + \frac{\operatorname{tr}\left(\tilde{W}^T\tilde{W}\right)}{2\gamma_\Delta} + \frac{\tilde{D}^T\tilde{D}}{2\gamma_D} \tag{39}$$

where $\gamma_\Delta \in \mathbb{R}^+$ and $\gamma_D \in \mathbb{R}^+$ are design constants, and $k_{p_\omega} \in \mathbb{R}^+$ denotes the composite gain. Under the assumption that $\dot{\tilde{W}} \approx \dot{\hat{W}}$, the time derivative of V_ω is expressed as:

$$\begin{aligned}\dot{V}_\omega &= \varepsilon_\omega^T\dot{\varepsilon}_\omega + k_{p_\omega}\tilde{\omega}_{BL}^T\dot{\tilde{\omega}}_{BL} + \frac{\operatorname{tr}\left(\tilde{W}^T\dot{\hat{W}}\right)}{\gamma_\Delta} + \frac{\tilde{D}^T\dot{\hat{D}}}{\gamma_D}\\ &= \varepsilon_\omega^T\zeta_\omega\left(f + gu + \Delta + D - \dot{\omega}_d - \dot{\upsilon}_\omega + \ell_\omega\right)\\ &+ \frac{\operatorname{tr}\left(\tilde{W}^T\dot{\hat{W}}\right)}{\gamma_\Delta} + \frac{\tilde{D}^T\dot{\hat{D}}}{\gamma_D} + k_{p_\omega}\tilde{\omega}_{BL}^T\Big(\tilde{\Delta} + \tilde{D} - k_{e_\omega}\tilde{\omega}_{BL}\\ &- k_{e_\omega}\tilde{\omega}_{BL}^{\lceil\eta_1\rfloor} - k_{e_\omega}\tilde{\omega}_{BL}^{\lceil\eta_2\rfloor}\Big)\end{aligned} \tag{40}$$

where $\dot{\upsilon}_\omega$ is obtained using Equation (24). By employing the σ-modification technique, the terms $\dot{\hat{W}}$ and $\dot{\hat{D}}$ are defined as follows:

$$\dot{\hat{W}} = \gamma_\Delta\mu\left(\varepsilon_\omega^T\zeta_\omega^T - k_{p_\omega}\tilde{\omega}_{BL}^T\right) - \sigma_\Delta\hat{W} \tag{41a}$$

$$\dot{\hat{D}}_{\omega_e} = \gamma_D\left(\zeta_\omega\varepsilon_\omega - k_{p_\omega}\tilde{\omega}_{BL}\right) - \sigma_D\hat{D} \tag{41b}$$

where $\sigma_\Delta \in \mathbb{R}^+$ and $\sigma_D \in \mathbb{R}^+$ are design constants. Upon substituting these expressions, in conjunction with Equation (26), the time derivative of V_ω simplifies to the following form:

$$\begin{aligned}\dot{V}_\omega \le &- k_\omega\varepsilon_\omega^T\varepsilon_\omega - k_{p_\omega}k_{e_\omega}\tilde{\omega}_{BL}^T\tilde{\omega}_{BL} - \frac{\sigma_\Delta}{\gamma_\Delta}\operatorname{tr}\left(\tilde{W}^T\hat{W}\right)\\ &- \frac{\sigma_D}{\gamma_D}\tilde{D}^T\dot{D}_\omega - \frac{\sigma_D}{\gamma_D}\tilde{D}^T\hat{D}\end{aligned} \tag{42}$$

Using the definition of $\tilde{W}$, we obtain:

$$-\frac{\sigma_\Delta}{\gamma_\Delta}\operatorname{tr}\left(\tilde{W}^T\hat{W}\right) \le -\lambda_\Delta\operatorname{tr}\left(\tilde{W}^T\tilde{W}\right) + \kappa_\Delta\operatorname{tr}\left(W^TW\right) \tag{43}$$

where $\lambda_\Delta = -\frac{\sigma_\Delta}{\gamma_\Delta}\left(1 - \frac{\delta_\Delta}{2}\right)$ with $\delta_\Delta \in \mathbb{R}^+$ and $\delta_\Delta < 2$, and $\kappa_\Delta = \frac{\sigma_\Delta}{2\gamma_\Delta\delta_\Delta}$. Similarly, using the definition of $\tilde{D}$, we have:

$$-\frac{\sigma_D}{\gamma_D}\tilde{D}^T\left(\hat{D} + \dot{D}\right) \le -\lambda_D\tilde{D}^T\tilde{D} + \kappa_D\acute{D}^T\acute{D} \tag{44}$$

where $\lambda_D = -\frac{\sigma_D}{\gamma_D}\left(1 - \frac{\sigma_D}{2}\right)$, with $\delta_D \in \mathbb{R}^+$ and $\delta_D < 2$, and $\kappa_D = \frac{\sigma_D}{2\gamma_D\delta_D}$, both of which are positive constants. Moreover, $\acute{D} = D^m + \dot{D}^m$. By substituting Equations (43) and (44) into Equation (42), the expression for $\dot{V}_2$ is subsequently simplified as:

$$\dot{V}_\omega \le -k_\omega' V_\omega + c_\omega \tag{45}$$

where $k_\omega' = \min\left(2k_\omega, 2\gamma_\Delta\lambda_\Delta, 2\gamma_D\lambda_D, 2k_{e_\omega}\right)$, and $c_\omega = \kappa_\Delta\operatorname{tr}\left(W^TW\right) + \kappa_D\acute{D}^T\acute{D}$. From the resulting expression, it can be concluded that ε_ω remains bounded. Since ε_ω is bounded, it follows that e_{ω_e} is also bounded within the specified upper and lower bounds. As a result, this implies the boundedness of q_e. Therefore, the boundedness of all system states is guaranteed, thereby completing the proof.

The block diagram of the proposed control method is presented in Figure 1.

5. SIMULATION RESULTS

5.1 Tracking Desired Euler Angles

The efficacy of the proposed control method is demonstrated through numerical simulations in this subsection. The reference frame used in the simulation is the local-vertical-local-horizon (LVLH) frame, where $\omega_r = \begin{bmatrix}0 & -n & 0\end{bmatrix}^T$, with $n = \sqrt{\mu_e/r_s^3}$ for a circular orbit. In this context, μ_e represents the gravitational constant of the Earth, and r_s denotes the

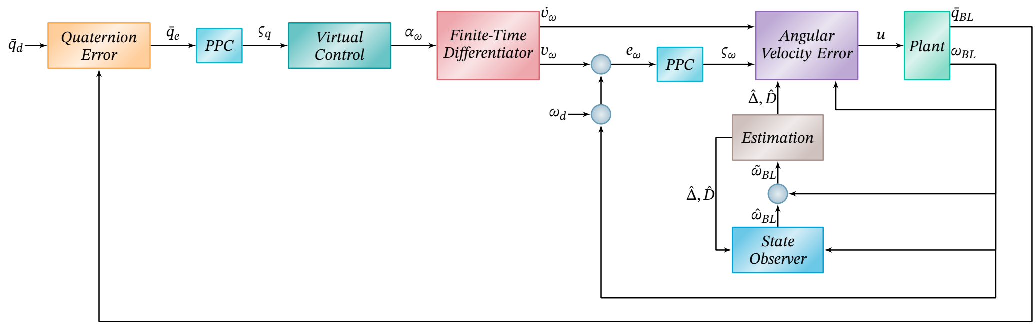

Fig. 1. Closed-loop block diagram of the proposed control system.

distance from the spacecraft to the Earth's center. Moreover, the external disturbances from aerodynamic drag and gravity gradient are modeled as per the methodology in Baldi et al. (2019). For a circular orbit, the parameter ω_r remains constant ($\dot{\omega}_r = 0_{3\times1}$). The parameters used in the simulation are summarized in Table 1. In addition, the initial value of the parameters are set to zero.

Table 1. Simulation and control parameters.

	Parameter	Value
Spacecraft	J_0 [kg.m^2]	$\begin{bmatrix} 20 & 1.2 & 0.9 \\ 1.2 & 17 & 1.4 \\ 0.9 & 1.4 & 15 \end{bmatrix}$
	ΔJ [kg.m^2]	$0.1J_0 + \mathrm{rand}\,(3,3)$
	Orbit	circular
	h [km]	350
	C_D	2.2
	r_{cp} [m]	$\begin{bmatrix}0.1 & 0.1 & -0.1\end{bmatrix}^T$
	$\omega_{BL}(0)$ [rad/s]	$\begin{bmatrix}0.2 & -0.2 & -0.1\end{bmatrix}^T$
Control	$\theta_d(t)$ [rad]	$\begin{bmatrix} -0.35\cos\left(\frac{\pi t}{20}\right) \\ -0.45\cos\left(\frac{\pi t}{25}\right) \\ +0.55\cos\left(\frac{\pi t}{30}\right) \end{bmatrix}$
	$(k_q, k_\omega, k_{p_\omega}, k_{e_\omega})$	$(0.25, 4, 5, 3)$
FD	(R, a_1, a_2)	$(10, 0.2, 0.5)$
NN/DO	$(\gamma_\Delta, \gamma_D, \sigma_\Delta, \sigma_D)$	$(5, 5, 10^{-5}, 10^{-5})$
	NN Neurons	50
	NN Centers	$\in [-3, 3]$
	NN Widths	$\in [3, 5]$
PF	T [s]	10 s
	$\left(m_q, n_q, p_q, r_q, \rho_q(0), \rho_{\infty_q}\right)$	$(13, 5, 7, 9, 0.5, 0.01)$
	$\left(m_\omega, n_\omega, p_\omega, r_\omega, \rho_\omega(0), \rho_{\infty_\omega}\right)$	$(19, 5, 7, 9, 0.25, 0.01)$

Remark 3. The total uncertainty, which is estimated through the combined neural network and disturbance observer, is defined by the following relation:

$$\Lambda = \Delta + D \tag{46}$$

Figure 2 presents the time history of quaternion errors. As shown, the proposed control system successfully maintains the quaternion errors within permissible bounds and drives them to zero, despite the presence of modeling uncertainties and external disturbances. Figure 3 illustrates the evolution of Euler angles, indicating that the desired attitude is accurately tracked within the specified time frame. Figure 4 displays the time history of angular velocity errors, further demonstrating the controller's effectiveness in keeping the errors within acceptable limits and eliminating them as intended. Figure 5 shows both the actual and desired angular velocities between body and reference frames, confirming accurate tracking within the designated time. Figure 6 depicts the control torques required to achieve the desired maneuver. Lastly, Figure 7 illustrates the time history of the estimated cumulative uncertainty, showing that the integration of the neural network and disturbance observer—enhanced through a joint training strategy—enables the system to estimate cumulative uncertainties with high accuracy.

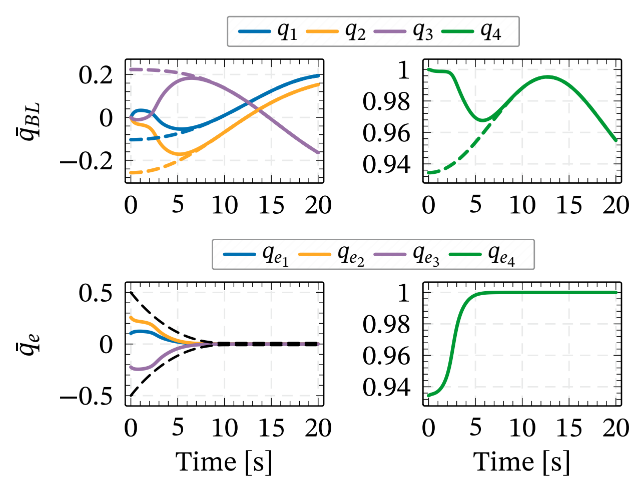

Fig. 2. Time history of the quaternions and their corresponding errors (black dashed lines represent error bounds and colored dashed lines represent the desired values of quaternions).

5.2 Comparison with Existing Methods

To provide a more detailed evaluation of the proposed control method's effectiveness, a comparison is conducted between the the suggested approach and the methodology outlined in Xie et al. (2022). The regulation-to-zero scenario replicates that of Xie et al. (2022), with the exception that

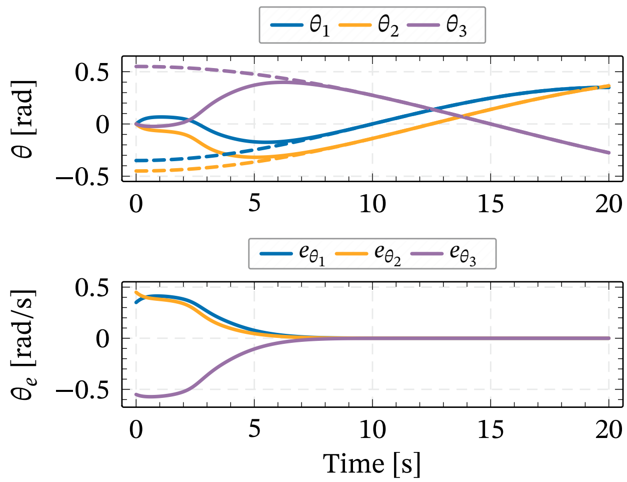

Fig. 3. Time history of the Euler angles and their corresponding errors (colored dashed lines represent the desired values of Euler angles).

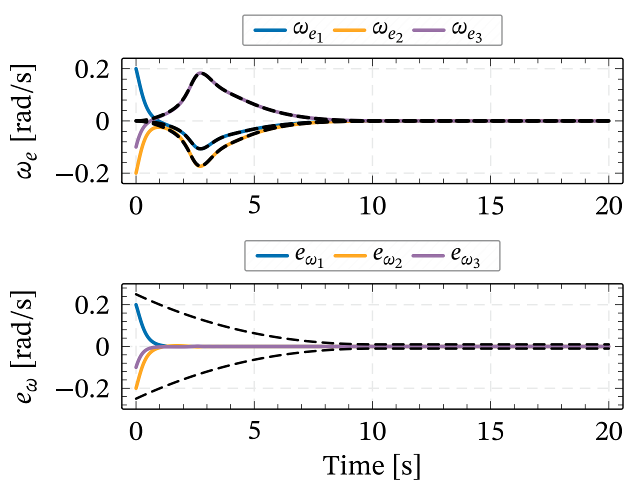

Fig. 4. Time history of angular velocity errors (black dashed lines in the first row represent desired values and represent error bound in the second row).

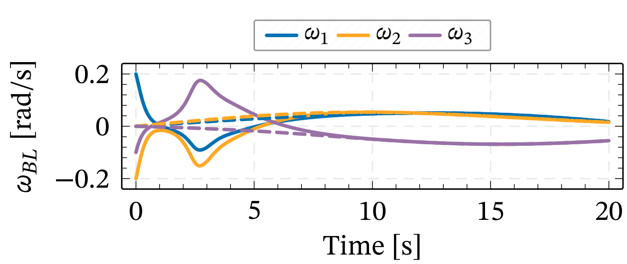

Fig. 5. Time history of angular velocities between body and reference frames.

the external disturbances described in that study have been modified as below:

$$d = \left(\|\omega_{rel}\|^2 + 0.2\right)\left[\sin(0.8t)\ \cos(0.5t)\ \sin(0.3t)\right]^T \quad (47)$$

To quantitatively compare the performance of two methods, the Mean Absolute Tracking Error (MATE) and Control Effort (CE) are employed as key evaluation metrics:

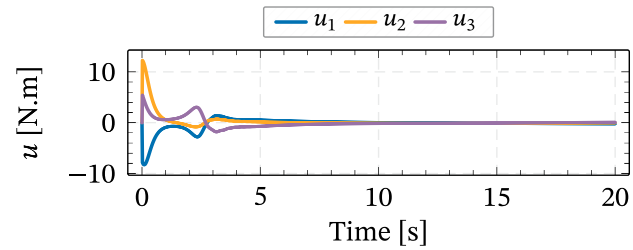

Fig. 6. Time history of required control torques.

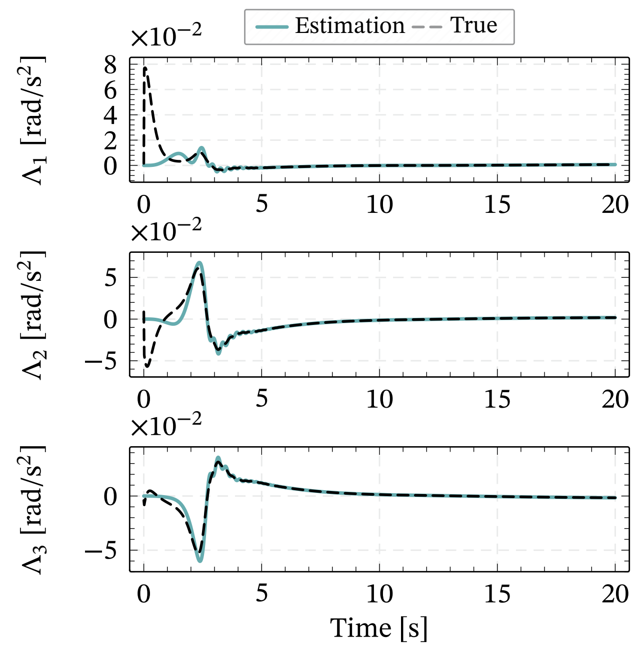

Fig. 7. Time history of estimation of total uncertainties.

$$\text{MATE} = \frac{1}{T_s}\int_0^{T_s} \|q_{BL}\|\text{d}t\ ,\ \text{CE} = \frac{1}{T_s}\int_0^{T_s} \|u\|\text{d}t \quad (48)$$

Table 2 presents the values corresponding to these parameters. As observed, the method introduced in Xie et al. (2022), owing to its use of predefined-time stability, exhibits a lower MATE throughout the entire time interval. However, in the proposed method, due to the system's requirement to reach the permissible error bound within a specified time, the overall accumulated error is higher. Nonetheless, when the error is evaluated after 8 seconds, it becomes evident that the tracking error during the steady-state phase in the proposed method is significantly lower than that of the approach in Xie et al. (2022). Moreover, the control effort required to achieve the control objective in the proposed method is less than that of the method in Xie et al. (2022). These results demonstrate the superiority of the method presented in this paper.

Table 2. Comparison of MATE and CE between the proposed method and the benchmark method.

Method	**MATE**	**MATE ($t \geq 8$)**	**CE [N.m]**
Proposed	0.1276	9.232×10^{-5}	1.976
Xie et al. (2022)	0.02373	0.001901	5.54

6. CONCLUSION

In this study, the prescribed performance of a spacecraft was investigated under the influence of modeling uncertainties and external disturbances. A novel performance function, grounded in the fixed-time stability framework, was introduced. Using the backstepping approach, a prescribed performance control strategy for the spacecraft was designed. To address the term explosion issue commonly associated with backstepping, a finite-time differentiator was employed. Additionally, a combination of a neural network and a disturbance observer was used to compensate for model uncertainties and external disturbances. Simulation results demonstrated that the proposed control method effectively eliminated tracking errors in quaternions and angular velocities within the desired time frame. Furthermore, the integration of the neural network and disturbance observer, coupled with a composite learning method, facilitated accurate estimation of unknown parameters.

REFERENCES

Baldi, P., Blanke, M., Castaldi, P., Mimmo, N., and Simani, S. (2019). Fault diagnosis for satellite sensors and actuators using nonlinear geometric approach and adaptive observers. *International Journal of Robust and Nonlinear Control*, 29(16), 5429–5455.

Bechlioulis, C.P. and Rovithakis, G.A. (2008). Robust adaptive control of feedback linearizable mimo nonlinear systems with prescribed performance. *IEEE Transactions on Automatic Control*, 53(9), 2090–2099.

Bhat, S.P. and Bernstein, D.S. (2000). Finite-time stability of continuous autonomous systems. *SIAM Journal on Control and optimization*, 38(3), 751–766.

Bu, X., He, G., and Wei, D. (2018). A new prescribed performance control approach for uncertain nonlinear dynamic systems via back-stepping. *Journal of the Franklin Institute*, 355(17), 8510–8536.

Doruk, R.Ö. (2008). Nonlinear controller designs for a reaction wheel actuated observatory satellite.

Emami, S.A., Banazadeh, A., Hajipourzadeh, P., Castaldi, P., and Fazelzadeh, S.A. (2023). Disturbance observer-based adaptive neural guidance and control of an aircraft using composite learning. *Control Engineering Practice*, 134, 105463.

Ezabadi, M. and Emami, S.A. (2024). Finite-time fault-tolerant control of a spacecraft using composite learning in the presence of moment of inertia uncertainty and external disturbances. *Aerospace Science and Technology*, 150, 109185.

Farrell, J.A., Polycarpou, M., Sharma, M., and Dong, W. (2009). Command filtered backstepping. *IEEE Transactions on Automatic Control*, 54(6), 1391–1395.

Gao, S., Liu, X., Jing, Y., and Dimirovski, G.M. (2021a). Finite-time prescribed performance control for spacecraft attitude tracking. *IEEE/ASME Transactions On Mechatronics*, 27(5), 3087–3098.

Gao, S., Liu, X., Jing, Y., and Dimirovski, G.M. (2021b). A novel finite-time prescribed performance control scheme for spacecraft attitude tracking. *Aerospace Science and Technology*, 118, 107044.

Golestani, M., Mobayen, S., ud Din, S., El-Sousy, F.F., Vu, M.T., and Assawinchaichote, W. (2022). Prescribed performance attitude stabilization of a rigid body under physical limitations. *IEEE Transactions on Aerospace and Electronic Systems*, 58(5), 4147–4155.

Guan, T., Zhang, K., Tan, S., and Li, B. (2023). Event-triggered attitude tracking control of spacecraft formation with prescribed performance. In *2023 2nd Conference on Fully Actuated System Theory and Applications (CFASTA)*, 992–997. IEEE.

Gui, M., Dai, M.Z., Zhang, C., Zhang, X., and Wu, J. (2024). Prescribed performance spacecraft attitude control with multiple convergence rates. *Symmetry*, 16(7), 789.

Horri, N.M. and Palmer, P. (2012). Practical implementation of attitude-control algorithms for an underactuated satellite. *Journal of Guidance, Control, and Dynamics*, 35(1), 40–45.

Hu, Q., Shao, X., and Guo, L. (2017a). Adaptive fault-tolerant attitude tracking control of spacecraft with prescribed performance. *IEEE/ASME Transactions On Mechatronics*, 23(1), 331–341.

Hu, Q., Shao, X., and Guo, L. (2017b). Adaptive fault-tolerant attitude tracking control of spacecraft with prescribed performance. *IEEE/ASME Transactions On Mechatronics*, 23(1), 331–341.

Hu, Y., Geng, Y., Wu, B., and Wang, D. (2020). Model-free prescribed performance control for spacecraft attitude tracking. *IEEE Transactions on Control Systems Technology*, 29(1), 165–179.

Liu, Q.Z., Zhang, L., Sun, B., Xiao, Y., and Fan, G.W. (2024). Fixed-time disturbance observer-based attitude prescribed performance predictive control for flexible spacecraft. *IEEE Transactions on Aerospace and Electronic Systems*.

Luo, J., Yin, Z., Wei, C., and Yuan, J. (2018). Low-complexity prescribed performance control for spacecraft attitude stabilization and tracking. *Aerospace Science and Technology*, 74, 173–183.

Ma, K. (2012). Comments on “quasi-continuous higher order sliding-mode controllers for spacecraft-attitude-tracking maneuvers”. *IEEE Transactions on Industrial Electronics*, 60(7), 2771–2773.

Polyakov, A. (2011). Nonlinear feedback design for fixed-time stabilization of linear control systems. *IEEE transactions on Automatic Control*, 57(8), 2106–2110.

Shao, X., Hu, Q., Shi, Y., and Jiang, B. (2018). Fault-tolerant prescribed performance attitude tracking control for spacecraft under input saturation. *IEEE Transactions on Control Systems Technology*, 28(2), 574–582.

Xiang, Y., Bing, X., Qingbin, G., and Xuebo, Y. (2019). Advanced control design and its application to aerospace mechatronics.

Xie, S., Chen, Q., and He, X. (2022). Predefined-time approximation-free attitude constraint control of rigid spacecraft. *IEEE Transactions on Aerospace and Electronic Systems*, 59(1), 347–358.

Yao, Q. (2021). Robust finite-time control design for attitude stabilization of spacecraft under measurement uncertainties. *Advances in Space Research*, 68(8), 3159–3175.

Zuo, Z. (2015). Non-singular fixed-time terminal sliding mode control of non-linear systems. *IET control theory & applications*, 9(4), 545–552.

Zuo, Z., Tian, B., Defoort, M., and Ding, Z. (2017). Fixed-time consensus tracking for multiagent systems with high-order integrator dynamics. *IEEE Transactions on Automatic Control*, 63(2), 563–570.